Journal of Magnetism and Magnetic Materials 587 (2023) 171327

Contents lists available at ScienceDirect

Journal of Magnetism and Magnetic Materials

journal homepage: www.elsevier.com/locate/jmmm

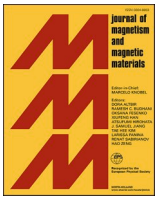

Structural and magnetic properties of Sb substituted LTP Mn-Bi annealed ribbons

Minkyu Kang [a], Hansol Lee [a], Jihoon Park [b,*], Jongryoul Kim [a,*]

[a] Department of Materials Science and Chemical Engineering, Hanyang University, Ansan 15588, Republic of Korea
[b] Powder Materials Division, Korea Institute of Materials Science, Changwon, Gyeongsangnam-do 51508, Republic of Korea

ARTICLE INFO

Keywords:
LTP Mn-Bi
Rare-earth free
Permanent magnet
Melt-spinning
Magnetic properties

ABSTRACT

We optimized the composition of Mn-Bi alloy, examined the effects of third element substitution of Sn, Cu, Al, and Sb on the magnetic properties, and investigated the microstructures and magnetic properties of Sb substituted Mn-Bi annealed ribbons. The optimized composition was $Mn_{54}Bi_{46}$, and it was found that the Sb substitution had the most positive effects on the magnetic properties among the substitution elements. Thus, we accomplished a detailed investigation on $Mn_{54}Bi_{46-x}Sb_x$ ($0.0 \leq x \leq 5.0$) annealed ribbons. The fracture planes of the annealed ribbons revealed that the grain size drastically decreased from a few tens of microns to submicrons close to the single domain size, which substantially enhanced the coercivity (H_c), remanent magnetization (M_r), and maximum energy product ($(BH)_{max}$). As a result, as the Sb content changed from 0 to 1.5, the M_r, H_c, and $(BH)_{max}$ of randomly oriented samples increased significantly from 14.7 emu/g, 0.50 kOe, and 0.15 MGOe to 37.2 emu/g, 8.15 kOe, and 3.27 MGOe, respectively. Furthermore, the temperature dependence of H_c on the Sb substitution showed significant enhancement over a wide temperature range from 223 to 378 K, suggesting that Mn-Bi alloy can be used in electrical vehicles.

1. Introduction

As interest and demand for electric vehicles are rapidly increasing for the reduction of greenhouse gas emission, the replacement of oil and natural gas with renewable energy, and the need for carbon neutrality, the weight reduction and miniaturization of motors is critical to improve the performance of electric vehicles. Accordingly, as one of the key materials that can increase the efficiency of motors, the demand for permanent magnet materials is explosively increasing. Currently, ferrite and Nd-based permanent magnets are the most widely used magnets in industry. Ferrite magnets are inexpensive to manufacture and have excellent thermal/chemical stability, but they have relatively low magnetic properties. On the contrary, Nd-based permanent magnets have very high magnetic properties, but have low thermal/chemical stability, high price, geographical concentration of rare earth elements, and political and strategic export restrictions. This dualization of the market exists because there is no permanent magnet material that can compromise the price and performance between ferrite and Nd-based magnets. Nd-based magnets have been widely used in high performance applications such as electric vehicles and wind turbines, but recently the demand for Nd-based magnets in consumer electronics such as cell phones, industrial motors, and power tools has also increased, which may lead to supply shortages. The availability of substitutes (gap-magnets) for intermediate performance grades in the supply chain of the magnet market can reduce the concentrated pressure on rare earth resources. Magnets with these intermediate characteristics are called 'gap-magnets', and their development is in strong demand [1].

Among permanent magnet materials, intermetallic low-temperature phase (LTP) Mn-Bi is of high scientific and technological interest as a candidate for a 'gap-magnet' that can fill the gap between ferrite and Nd-based magnets. LTP Mn-Bi has a higher theoretical maximum energy product $(BH)_{max}$ of around 20 MGOe at room temperature [2,3] than ferrite of ~ 4 MGOe without using rare-earth elements, and has higher H_c than Nd-based magnets at high temperatures due to the positive temperature coefficient of H_c [4,5]. This positive temperature coefficient of H_c is favorable for high-temperature applications, but disadvantageous for low-temperature applications due to the decrease of H_c in the lower operating temperature range of electronic devices, which limits the use of LTP Mn-Bi.

Up to now, many researches on substitution/doping of a third element in the binary LTP Mn-Bi for the enhancement of H_c at low temperature have been extensively conducted through computational

* Corresponding authors.
E-mail addresses: jpark@kims.re.kr (J. Park), jina@hanyang.ac.kr (J. Kim).

https://doi.org/10.1016/j.jmmm.2023.171327
Received 29 June 2023; Received in revised form 14 September 2023; Accepted 26 September 2023
Available online 7 October 2023

and experimental studies. In computational simulation approaches, crystal structures of Fe, Co, Nd, Si, Al, Pt, Sn, and/or Sb substituted/doped Mn-Bi were calculated for magnetic moment (M), anisotropy constant (K), and $(BH)_{max}$ using first-principle calculations [2,6–12]. Experimentally, there have been studies on the third element substituted/doped thin film, powder, and bulk using sputtering, ingot manufacturing, melt-spinning, annealing, powdering, and sintering processes [13–21]. In particular, the melt-spinning process has been heavily used in LTP Mn-Bi research to enhance the phase purity [22–24]. Since the difference in melting points between Mn (1245 °C) and Bi (271 °C) is too large and a peritectic reaction is required to form the LTP phase, it is difficult to obtain a high-purity LTP Mn-Bi phase by conventional melting processes.

Sakuma *et al.* reported a theoretical study in which the small negative K of Mn-Bi changed to the large positive value of 2×10^6 K/m^3 when substituting Sn for Bi [8]. Through computational simulation, Choi *et al.* expected that the low temperature properties of Mn-Bi could be improved by doping Mn-Bi with Cu to increase the peritetic reaction temperature of the LTP Mn-Bi phase [11]. Yang *et al.* fabricated a Sn doped LTP Mn-Bi magnet and reported that the H_c was improved by forming an intergranular phase for isolating LTP Mn-Bi grains [13]. Ramakrishna *et al.* found that the decomposition of LTP Mn-Bi during a ball milling process could be reduced by adding Al and Cu [14]. Gabay *et al.* reported that when Sb was substituted in MnBi, a quenched high-temperature phase (QHTP) was formed in the melt-spun ribbon with H_c over 20 kOe at room-temperature. Furthermore, it was found that the LTP Mn-Bi retaining high H_c was obtained after subsequent heat-treatment [25].

The above results show that Mn-Bi alloy can be a good candidate for a gap magnet. However, it was reported that the H_c sharply decreases to less than 1 kOe at 223 K [40]. This indicates that it is still required to increase the low temperature H_c for application to electrical vehicles. Therefore, we aimed to develop a suitable ternary Mn-Bi-Z alloy with an excellent H_c value in the practical operation temperature range. We firstly optimized the composition of binary Mn-Bi alloys through common processing methods, such as arc-melting, melt-spinning, and annealing processes. To improve the thermal and magnetic properties, the effects of various heterogeneous elements, i.e., Sn, Cu, Al, and Sb, were examined. It was found that the grain refinement was well developed when Bi was replaced with Sb. We studied the crystallographic, microstructural, and magnetic properties by subdividing the Sb concentration in Mn-Bi, i.e., $Mn_{54}Bi_{46-x}Sb_x$ ($0.0 \leq x \leq 5.0$). As a result, the magnetic properties of the Sb substituted LTP Mn-Bi were measured to confirm their performance in a wide temperature range between 223 and 378 K for practical electronic applications.

2. Experimental method

Mn_xBi_{100-x} ($x = 48$, 50, 52, 54, 56, 58, and 60) ribbons were prepared by arc-melting high purity Mn (99.9 %) and Bi (99.99 %) chips in an Ar atmosphere, followed by melt-spinning and annealing processes. The chips for each composition were mixed in the designated atomic ratios and placed on a copper hearth for the arc-melting. The arc-melted ingots were flipped and re-melted four times to ensure homogeneity. The fabricated ingots were then induction-melted in quartz nozzles with a 0.4 mm orifice and ejected onto a Cu wheel rotating at a tangential velocity of 50 m/s in an Ar atmosphere. The melt-spun ribbons were inserted into a horizontal tube furnace for annealing in an Ar atmosphere at temperatures ranging from 544 K, i.e., the melting temperature of Bi, to 613 K, i.e., the upper limit of the LTP crystallization temperature, for 24 hrs. The third element Z (=Sn, Cu, Al, and Sb) substituted Mn-Bi ribbons, i.e., Mn-Bi-Z, were fabricated with the same methods as the above Mn-Bi ribbons, but they were annealed at the optimized annealing temperature of 558 K. The purities of the substitution elements Sb, Sn, Al, and Cu were 99.9999 %, 99.99 %, 99.0 %, and 99.99 %, respectively.

An X-ray diffractometer (XRD, Rigaku D/MAS-2500/PC) with Cu Kα radiation ($\lambda = 1.54056$ Å) was used to analyze the crystal structure of the annealed Mn-Bi and Mn-Bi-Z ribbons, and the relative weight fraction and lattice parameter were calculated using Rietveld refinement by the JADE 9.5 program (Materials Data, Inc.) [26,27]. The morphology and microstructure of the annealed ribbons were observed by field emission scanning electron microscopy (FE-SEM, TESCAN, Czech, MIRA3). The elemental compositions of the annealed ribbons were analyzed by transmission electron microscopy (TEM, JEM-2100F, JEOL, Japan) and energy-dispersive X-ray spectroscopy. A vibration sample magnetometer (VSM, Lakeshore, 7410, USA) with a maximum field of 2.5 T at 300 K and SQUID-VSM (Quantum Design MPMS-3) with a maximum applied field of 5 T at 223, 248, 298, and 378 K were used to measure the magnetic properties of the samples. For the magnetic property measurement, the annealed ribbons were gently crushed with a mortar and pestle, and packed with paraffin wax in to cup-shaped Cu holders without any additional magnetic alignment process. The $(BH)_{max}$ of the annealed ribbons were evaluated using their density using their lattice parameters measured by XRD and their compositions based on the theoretical value.

3. Results and discussion

3.1. Composition optimization of binary Mn-Bi

Prior to the investigation of the third element substituted Mn-Bi alloy, the composition of the Mn-Bi binary phase was optimized. Mn_xBi_{100-x} ($x = 48$, 50, 52, 54, 56, 58, and 60) melt-spun ribbons were fabricated and their magnetic properties and the weight fractions of the crystallized phases were characterized. Fig. 1 (a) shows the XRD patterns of the annealed Mn-Bi ribbons. According to the XRD patterns and weight fraction analyses, LTP Mn-Bi were the main phase in all the sample. It is evident that the LTP Mn-Bi with a NiAs-type hexagonal structure with lattice constant of $a = 4.29$ Å, $c = 6.12$ Å was formed after the annealing process. The weight fractions of LTP Mn-Bi obtained when the Mn concentration x was 48, 50, 52, 54, 56, 58, and 60 were 77.9, 78.6, 95.7, 100, 94.2, 92.3, and 88.0 wt%, respectively. And when Mn concentration x = 54, a single-phase LTP Mn-Bi sample was obtained. The weight fraction of the LTP Mn-Bi for the sample at $x = 48$ was 77.9 wt%, which increased to higher than 99 wt% at $x = 54$. And then, it started to decrease as the Mn concentration further increased. It is noted that peaks for residual Bi with hexagonal structure appeared in all samples, except for the sample at $x = 54$, and their concentration decreased as the amount of Mn increased as can be seen in Fig. 1 (a). For the samples with high Mn concentrations, i.e., $x = 56$ and 58, manganese oxide peaks were also observed due to the remaining Mn, which is susceptible to oxidation.

In Fig. 1(b), we present the weight fraction of LTP Mn-Bi alongside the magnetization at 2.5 Tesla ($M_{2.5\ T}$) as a function of Mn concentration. It is evident that as the Mn concentration increases up to $x = 54$, the weight fraction of LTP Mn-Bi also increases, resulting in a corresponding increase in $M_{2.5\ T}$. At Mn concentration $x = 54$, which contains the highest weight fraction of LTP Mn-Bi, the material exhibits its peak $M_{2.5\ T}$ property, measuring at 62.5 emu/g. However, when the Mn concentration surpasses $x = 54$, the weight fraction of LTP Mn-Bi starts to decrease, leading to a subsequent decline in $M_{2.5\ T}$ properties. This observation highlights the direct relationship between the weight fraction of LTP Mn-Bi, determined by the Mn concentration conditions, and its influence on the $M_{2.5\ T}$ property. According to the references [28], it was confirmed that an excess Mn is necessary to obtain the highest purity of LTP to combat the phase segregation of Mn from the melt during arc-melting and melt-spinning processes. Thus, it is reasonable that $Mn_{54}Bi_{46}$ showed the highest weight fraction of LTP and $M_{2.5\ T}$. Therefore, for further experiments with the third element substituted Mn-Bi, $Mn_{54}Bi_{46}$ was used as a standard binary Mn-Bi composition to enhance the magnetic properties.

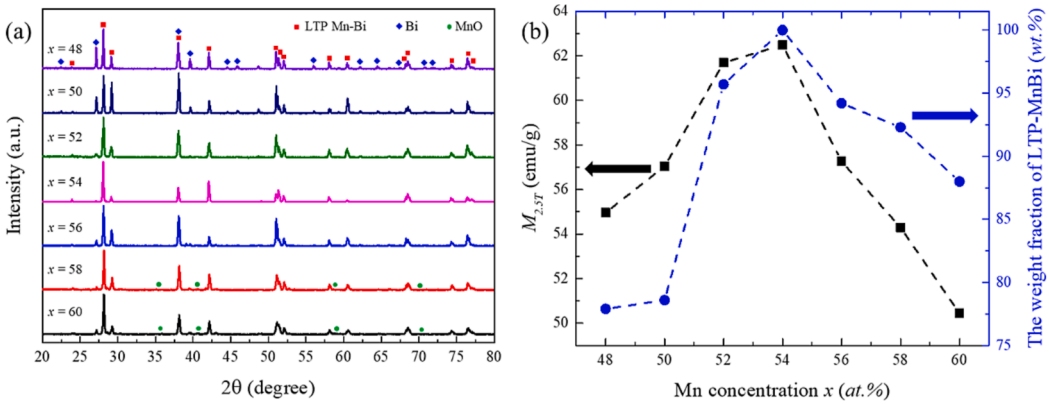

Fig. 1. Mn concentration (x) dependences of the (a) XRD patterns and (b) The weight fraction of LTP Mn-Bi and the magnetization at 2.5 Tesla ($M_{2.5\ T}$) for the Mn_xBi_{100-x} annealed ribbons at 558 K for 24 hrs.

3.2. Effects of third element substitutions into LTP Mn-Bi

As a third element to replace partial Bismuth, Sn, Cu, Al, and Sb were selected to improve the magnetic property, which exhibited positive results in the previous computational simulations and experimental studies [8,10–15,21]. In order to confirm the positive effects and systematically study the detailed magnetic properties, $Mn_{54}Bi_{46-x}Z_x$ melt-spun ribbons with a series of substitutional element concentrations (x) of 1, 3, and 5 *at.*% were fabricated with the same methods as the Mn-Bi binary ribbons. We calculated the lattice constants of the Mn-Bi samples substituted with Sn, Al, and Cu elements using the Rietveld refinement analysis. (The results have been summarized in the Table S1.) Fig. 2 shows the element concentration dependence of $M_{2.5\ T}$ and H_c for each composition. In $Mn_{54}Bi_{46-x}Sn_x$ annealed ribbons, no secondary phase was found in the XRD pattern (not shown here) of the sample at $x = 1$, but residual Bi was crystallized and peaks for antiferromagnetic Mn_3Sn with hexagonal structure [29] appeared as the Sn concentration increased. Accordingly, the corresponding $M_{2.5\ T}$ decreased from 60.5 to 57.7 emu/g as the Sn concentration increased from 0 to 3 *at.*%, while the H_c slightly increased from 0.4 to 1.1 kOe. The enhancement of H_c by the addition of Sn follows a trend similar to that in the previous studies [13]. Second, the Cu substituted Mn-Bi resulted in crystallization of a secondary $Bi_4Cu_{0.38}Mn_{3.41}$ phase based on its XRD analysis, thus reducing the proportion of the hard magnetic LTP Mn-Bi. The orthorhombic unit cell of $Bi_4Cu_{0.38}Mn_{3.41}$ phase is not ferromagnetic [30]. As the fractions of the LTP Mn-Bi and $Bi_4Cu_{0.38}Mn_{3.41}$ phases decreased and increased, respectively, the $M_{2.5\ T}$ dramatically decreased and H_c was enhanced with an increasing Cu concentration. Third, the Al substitution into LTP Mn-Bi resulted in a slight increase of $M_{2.5\ T}$ to 62.2 emu/g until $x = 1$, and then it gradually decreased with further increases of the Al concentration. The change of H_c in Fig. 2 (b) shows that the Al substitution had the least effect on the H_c among the candidate substituting elements. Last, the $Mn_{54}Bi_{46-x}Sb_x$ at $x = 1$ led to minor degradation of $M_{2.5\ T}$ and significant improvement of H_c as can be seen in Fig. 2 (a) and (b); the $M_{2.5\ T}$ decreased to 59.5 emu/g and H_c increased to 4.1 kOe. The trend of a dramatic increase in H_c with an increasing Sb concentration continued until $x = 3$, at which the H_c of 9.7 kOe was measured. From the above results from Sn, Cu, Al, and Sb substitutions into LTP Mn-Bi, we considered that Sb is the most effective element for H_c enhancement with a minor loss of $M_{2.5\ T}$. Therefore, we further investigated details of crystal structures, microstructures, and magnetic properties for the Sb substituted Mn-Bi.

3.3. Sb substitution into LTP Mn-Bi

3.3.1. Crystallographic properties of Sb substituted LTP Mn-Bi

We fabricated $Mn_{54}Bi_{46-x}Sb_x$ ($0.0 \leq x \leq 5.0$) annealed ribbons, and measured their crystallographic properties as shown in Fig. 3. In all the samples, no peaks for the residual Bi or manganese oxide were found. When the concentration of Sb in the LTP Mn-Bi was less than 1, i.e., x = 0.0 and 0.5, all the peaks analyzed by XRD were identified as LTP Mn-Bi, suggesting that all Sb atoms were incorporated into the lattice of LTP

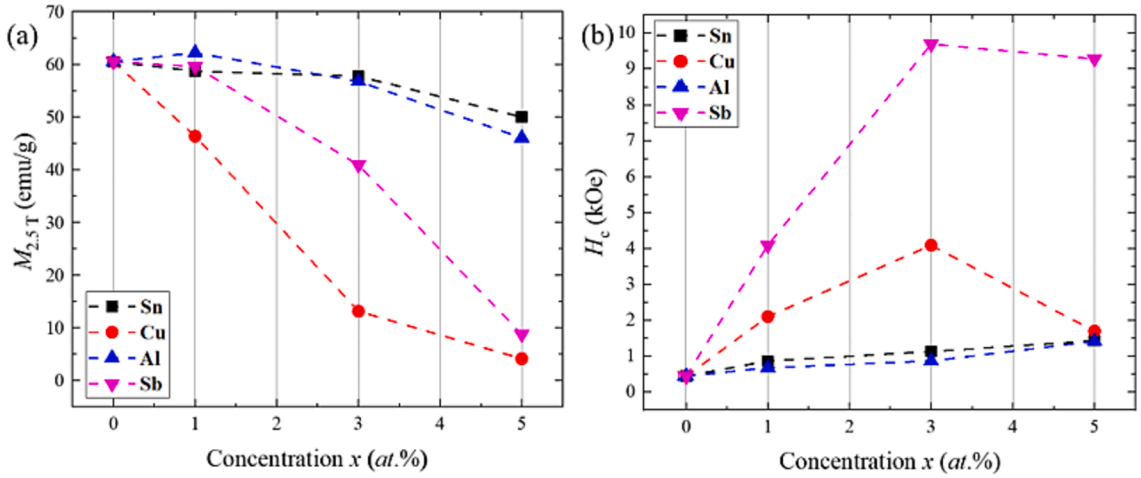

Fig. 2. Concentration (x) of substitution element (Z) dependences of (a) the magnetization at 2.5 Tesla ($M_{2.5\ T}$) and (b) coercivity (H_c) for the $Mn_{54}Bi_{46-x}Z_x$ (Z = Sn, Cu, Al, Sb, x = 0, 1, 3, 5) annealed ribbons.

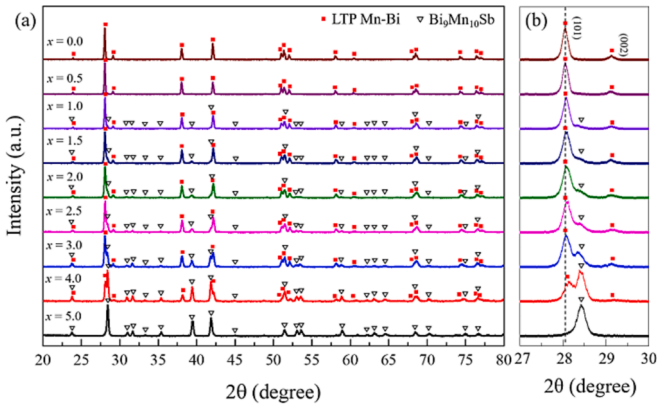

Fig. 3. XRD patterns of the $Mn_{54}Bi_{46-x}Sb_x$ ($0.0 \leq x \leq 5.0$) annealed ribbons.

Mn-Bi, while increasing peaks of the $Bi_9Mn_{10}Sb$ phase were detected as the Sb concentration was further increased. The $Bi_9Mn_{10}Sb$ phase is known to have antiferromagnetic properties in an orthorhombic structure ($P222_1$) [30–32]. However, there is also a research result that the $Bi_9Mn_{10}Sb$ compound exhibits ferromagnetism and substantial coercivity at below ~ 250 K [25]. The weight fraction of LTP Mn-Bi was still maintained at 83.7 % until $x = 1.5$, but then it decreased rapidly as the Sb concentration increased further, and only the $Bi_9Mn_{10}Sb$ phase was identified at $x = 5.0$. The phase transformation process from LTP Mn-Bi to $Bi_9Mn_{10}Sb$ phase with an increasing x can be observed in Fig. 3 (b). It is noteworthy that the (1 0 1) peak for LTP Mn-Bi was shifted from 28.042° to 28.122° when the Sb concentration increased from 0 to 4 due to the smaller atomic radius of Sb compared to that of Bi.

Fig. 4 shows the Sb concentration dependence of lattice parameters a and c, the c/a ratio, and the volume of the unit cell of $Mn_{54}Bi_{46-x}Sb_x$ ($0.0 \leq x \leq 5.0$) annealed ribbons. It is noted that the lattice parameters were averaged from the XRD patterns measured by three fabricated samples for each composition. The lattice parameters for $x = 0$ were $a = 4.2891$ Å, $c = 6.1235$ Å, and $c/a = 1.4277$, which are in good agreement with the previous research results of $a = 4.29$ Å, $c = 6.12$ Å, and $c/a = 1.4271$ [33]. The overall change of the lattice constants a and c was in the same direction. Upon substituting more Sb, there was continuous change in the lattice parameters with a and c becoming smaller, and finally decreasing to 4.2791 Å and 6.1136 Å, respectively, for $x = 3.0$. The only data point that did not follow the overall trend is the c at the Sb concentration of 0.5; the lattice constant c when $x = 0.5$ was increased to 6.1247 Å. We attributed the decreasing lattice constants to the smaller atomic radius of Sb than that of Bi, leading to shrinkage of the LTP Mn-Bi unit cell, as explained in the XRD analyses section above. The linearly decreasing trend for the lattice constants continued until $x = 2.0$ for c and $x = 2.5$ for a, and then began to slow down. Thus, the c/a ratio in the inset of Fig. 4 increased to 1.429 for $x = 2.0$, and then decreased to 1.4287 for $x = 3.0$. The trends of the lattice parameters a, c, unit cell volume, and c/a ratio of the annealed ribbons well agree with those of previous results for $MnBi_{1-x}Sb_x$ by computational simulations [34].

3.3.2. *Microstructures of Sb substituted LTP Mn-Bi*

To confirm the microstructural changes caused by the Sb substitution in the samples, we broke the $Mn_{54}Bi_{46-x}Sb_x$ ($x = 0.0$, 0.5, 1.0, and 3.0) annealed ribbons to observe the fracture planes and analyzed them with FE-SEM as shown in Fig. 5. As shown in the figure, the grains were revealed on the fractured surface. For the sample at $x = 0$, the grain size ranged from 10 to 20 μm, which is as large as the thickness of the annealed ribbons. When Sb of 0.5 *at.*% was added in the LTP Mn-Bi, the grain sizes shrank dramatically to 1.53 um. Further increasing the Sb concentration to 1.0 and 3.0 *at.*% decreased the average grain size to 0.95 and 0.36 μm, respectively, and also narrowed the size distribution as seen in Fig. 5. Under the condition of $x = 3.0$, the grain size reached the theoretical single domain size of the LTP Mn-Bi between 0.3 and 0.5 μm [35,36]. The increase in H_c with a decreasing grain size in the LTP Mn-Bi has been well documented in previous studies [37].

Fig. 6 shows a TEM micrograph and EDS elemental maps of the $Mn_{54}Bi_{44.5}Sb_{1.5}$ annealed ribbons for Mn, Bi, and Sb. As shown in the micrograph, fine dark colored crystallites were evenly distributed in the matrix. The elemental maps show that these fine crystallites had higher Mn concentration. On the contrary, Bi and Sb elements were uniformly distributed over the entire area, indicating that a non-magnetic intergranular phase [13,38], acting as a magnetic domain pinning site, was not developed. The XRD result in Fig. 3 confirmed that LTP Mn-Bi and $Bi_9Mn_{10}Sb$ phases coexisted in the annealed ribbons. This indicates that

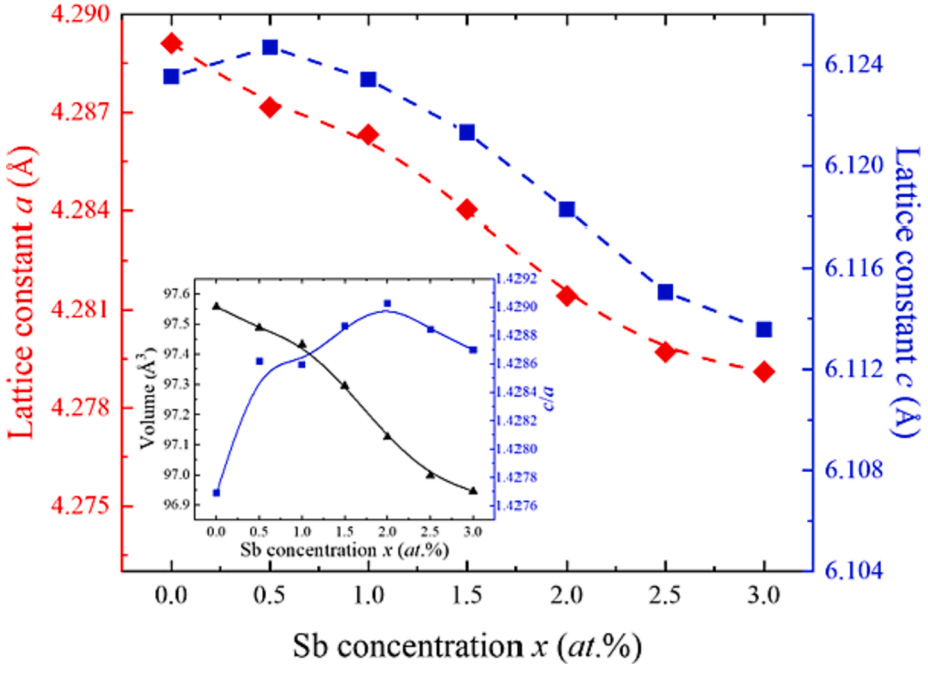

Fig. 4. Sb concentration (x) dependences of the lattice constants a and c, unit cell volume, and c/a ratio in the $Mn_{54}Bi_{46-x}Sb_x$ annealed ribbons.

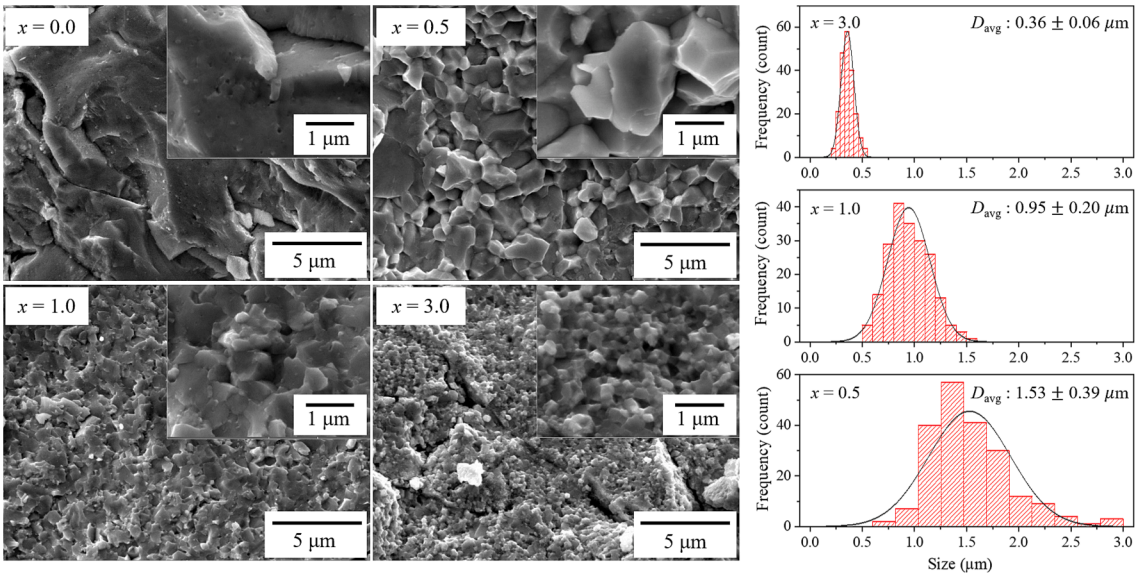

Fig. 5. FE-SEM images of the fractured planes and grain size distributions of the $Mn_{54}Bi_{46-x}Sb_x$ annealed ribbons (x = 0.0, 0.5, 1.0 and 3.0).

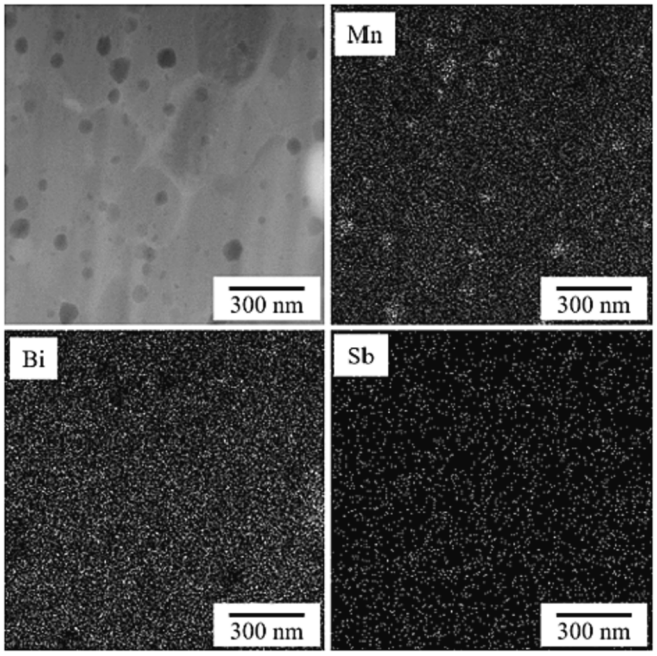

Fig. 6. A TEM micrograph and EDS elemental maps of the $Mn_{54}Bi_{44.5}Sb_{1.5}$ annealed ribbon.

the annealed ribbon consisted of LTP Mn-Bi grains ranging from 300 to 400 nm and ~ 60 nm sized Mn-rich phases embedded in the Mn-Bi matrix. This shows that the enhancement of the H_c by Sb substitution was strongly influenced by the grain refinement effect.

3.3.3. Magnetic properties of Sb substituted LTP Mn-Bi

VSM analysis was performed at room temperature to elucidate the effect of the Sb substitution on the magnetic properties. The measured hysteresis loops are shown in Fig. 7, and detailed $M_{2.5\ T}$, M_r, $M_r/M_{2.5\ T}$, H_c, and $(BH)_{max}$ are listed in Table 1. Fig. 7 (a) shows the magnetic hysteresis loops of the samples as a function of the Sb concentration, and the corresponding values are plotted in Fig. 7 (b). The measured hysteresis loop shows decrease the $M_{2.5\ T}$ and increase H_c as the content of x increases. This trend is attributed to the decrease of the magnetic phase, LTP Mn-Bi, and the increase of the antiferromagnetic phase, $Bi_9Mn_{10}Sb$. This is consistent with the fact that the main peak intensity of the $Bi_9Mn_{10}Sb$ phase increased significantly at x = 3 of Fig. 3. (b). Since the $Bi_9Mn_{10}Sb$ is an antiferromagnetic phase [30,31] that does not exhibit great magnetic properties, it has a significant effect on the reduction of magnetization, but has a limited effect on the kink of the hysteresis loops, as seen in Fig. 7.

The $M_{2.5\ T}$ of the Sb-free LTP Mn-Bi annealed ribbon was 62.5 emu/g, which was initially somewhat maintained with the increasing Sb concentration until x = 2, and then it rapidly decreased with a higher Sb concentration. The degree of degradation of the $M_{2.5\ T}$ with the Sb substitution was proportional to the fraction of the LTP replaced by the $Bi_9Mn_{10}Sb$ phase. In addition, the reduction of $M_{2.5\ T}$ was also caused by the magnetic moment decrease of Mn atoms. H. T. Nguyen, *et al.*, performed a density functional theory calculation on the Sb substituted LTP Mn-Bi and found that partial substitution of Sb for Bi reduced the magnetic moment of the Mn atom [34]. According to Fig. 4, the lattice constants a and c decreased with an increasing Sb concentration, which reduced the distance between the Mn atoms and increased the antiferromagnetic spin configuration, and thereby decreased the net magnetic moment.

The M_r of the Sb substituted LTP Mn-Bi at x = 0.5 substantially increased from 14.7 emu/g for x = 0.0 to 36.3 emu/g due to the dramatic enhancement of the H_c from 0.5 to 2.24 kOe. The M_r increased up to 37.3 emu/g for x = 1.0 and remained almost constant until x = 1.5, after which it began to decrease monotonically with an increasing Sb concentration. The initial enhancement of M_r was strongly related to the rise of H_c, while the latter monotonic decrease was caused by the drastic degradation of M_s. The H_c rapidly increased to 8.15 kOe for x = 1.5, then there was no further drastic change at the higher Sb concentrations. This H_c enhancement was attributed to the continued grain size refinement from several tens of microns for x = 0.0 to submicron for x = 0.5 as shown in Fig. 5. An additional reason for the enhanced H_c is that the c/a ratio increased until x = 2.0, and hence the magneto-crystalline anisotropy increased. The enhancement of the magnetic anisotropy of LTP Mn-Bi by the Sb substitution has also been noted in computational simulation studies. H. D. Qian *et al.* studied the effect of the Sb substitution for Bi in LTP Mn-Bi using first-principle calculations and found that the K value is dramatically enhanced from a small negative value (-0.85 MJ/m^3) to a large positive value (6.042 MJ/m^3) at 0 K [12]. A trend similar to that for M_r is seen for $(BH)_{max}$ with the Sb substitution in Fig. 7 (b). With the increasing Sb substitution concentration, the $(BH)_{max}$

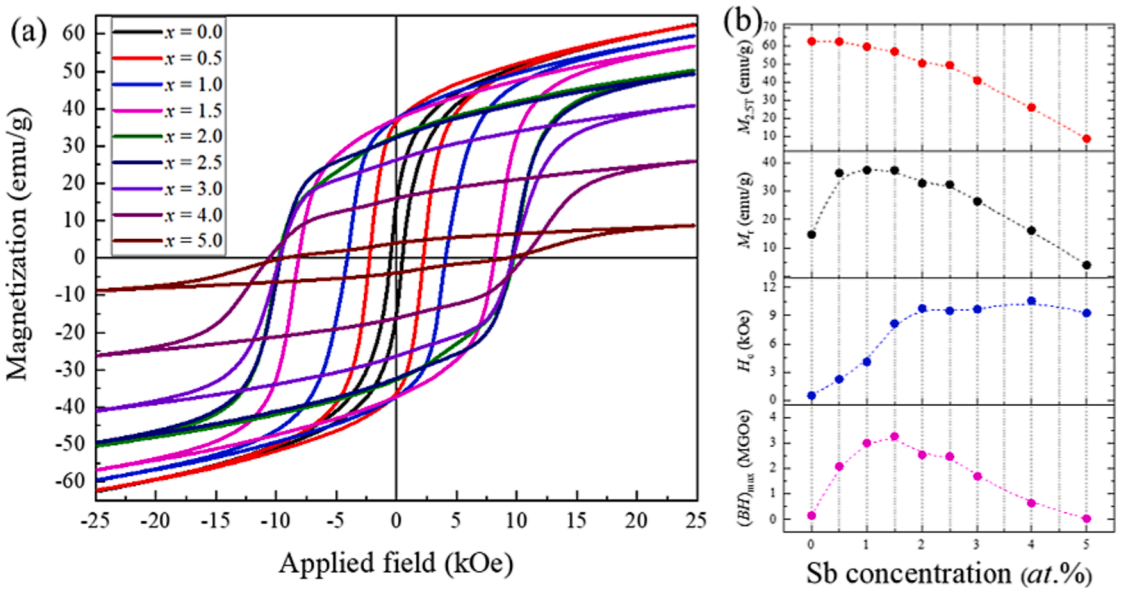

Fig. 7. Sb concentration (x) dependences of the (a) magnetic hysteresis loops and (b) magnetization at 2.5 Tesla ($M_{2.5\ T}$), remanent magnetization (M_r), coercivity (H_c), and maximum energy product $(BH)_{max}$ in the $Mn_{54}Bi_{46-x}Sb_x$ annealed ribbons.

Table 1
Magnetization at 2.5 Tesla ($M_{2.5\ T}$), remanent magnetization (M_r), squareness ($M_r/M_{2.5\ T}$), coercivity (H_c), and maximum energy product $(BH)_{max}$ in the $Mn_{54}Bi_{46-x}Sb_x$ annealed ribbons.

Sb concentration (x)	$M_{2.5\ T}$ (emu/g)	M_r (emu/g)	$M_r/M_{2.5\ T}$ (%)	H_c (kOe)	$(BH)_{max}$ (MGOe)
0.0	62.5	14.7	23.6	0.50	0.15
0.5	62.4	36.3	58.2	2.24	2.08
1.0	59.5	37.3	62.7	4.09	3.00
1.5	56.8	37.2	65.6	8.15	3.27
2.0	50.3	32.7	64.9	9.77	2.53
2.5	49.4	32.3	65.3	9.52	2.47
3.0	40.9	26.3	64.4	9.69	1.68
4.0	26.0	16.1	61.8	10.59	0.63
5.0	8.7	4.0	45.8	9.28	0.02

increased from 0.15 MGOe for the Sb-free sample to 3.27 MGOe for $x = 1.5$. Afterwards, with further increases of the Sb concentration, the $(BH)_{max}$ monotonically decreased to 0.02 MGOe for $x = 5.0$, according to the tendency of M_r.

The hysteresis loops of the four selected annealed ribbons, i.e., $Mn_{54}Bi_{46-x}Sb_x$ ($x = 0.0$, 1.0, 1.5, and 3.0), were measured at temperatures of 223, 248, 298 and 378 K to fully understand the temperature dependence of H_c according to the Sb concentration as shown in Fig. 8. The figure shows that the H_c of all samples increase as the temperature rises, since LTP Mn-Bi has a positive temperature coefficient of H_c, which originated from the increasing K of LTP Mn-Bi with temperatures from 150 to 530 K [4,39–41]. The H_c of the Sb-free annealed ribbon dramatically decreased from 2.89 to 0.27 kOe when the temperature decreased from 378 to 223 K. This indicates that the H_c measured at 223 K was reduced to less than 10 % compared to the value measured at 378 K. On the other hand, the Sb substitution resulted in a significant increase in H_c over the entire temperature range from 220 to 380 K as shown in Fig. 8. The H_c for $x = 1.5$ was 17.0 kOe and 4.1 kOe at 378 K (105 °C) and 248 K (-25 °C), respectively, where the temperatures were close to the highest and lowest temperatures that an electronic device can experience in daily life. Therefore, despite the degradation of the M_s and M_r, the above results demonstrate that the substitution of Sb into LTP Mn-Bi can significantly improve the magnetic properties over a wide temperature range.

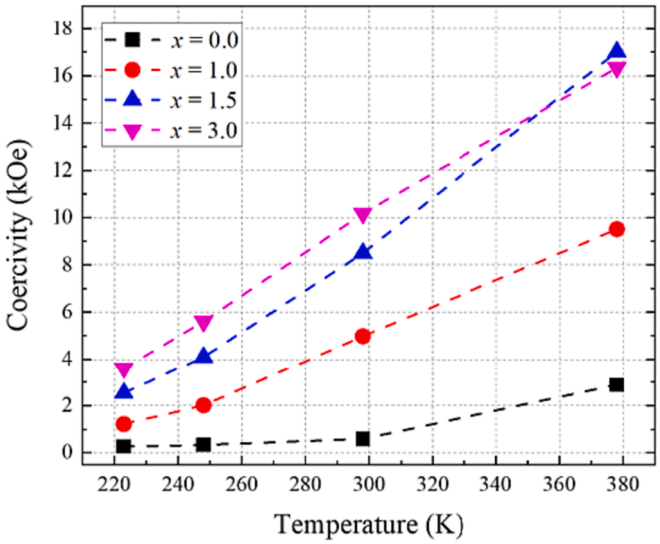

Fig. 8. Temperature dependences of coercivity (H_c) of the $Mn_{54}Bi_{46-x}Sb_x$ ($x = 0.0$, 1.0, 1.5, 3.0) annealed ribbons.

4. Conclusions

We first optimized the composition of Mn-Bi annealed ribbons, and then tested the Sn, Cu, Al, and Sb substitution effects on the Mn-Bi annealed ribbons for magnetic property enhancement. We concluded that the Sb substitution had the most positive effects on the enhancement of magnetic properties, and thus, we conducted a detailed investigation of Sb substitution effects, i.e., $Mn_{54}Bi_{46-x}Sb_x$ ($0.0 \leq x \leq 5.0$), on phase crystallizations, microstructures, and magnetic properties. We found the LTP to be the main phase in the annealed ribbons with $x \leq 0.5$, whereas the secondary $Bi_9Mn_{10}Sb$ phase began to appear at a higher x. Nevertheless, the remanent magnetization (M_r) increased significantly until around $x = 1.5$ due to the substantially enhanced coercivity (H_c) caused by microstructure refinement from a few tens of microns to submicrons approaching the single domain size of LTP Mn-Bi. The M_r, H_c, and maximum energy product $(BH)_{max}$ for $x = 1.5$ were 37.2 emu/g, 8.15 kOe, and 3.27 MGOe, respectively, which were considerably

increased from 14.7 emu/g, 0.50 kOe, and 0.15 MGOe for the Sb-free sample. The fabricated Sb substituted Mn-Bi also exhibited enhanced temperature dependence of H_c over a temperature range from 223 to 378 K. Accordingly, our study confirmed that the Sb substituted Mn-Bi is a potential rare-earth free permanent magnetic material over the wide temperature range that practical electronic devices can experience.

CRediT authorship contribution statement

Minkyu Kang: Conceptualization, Investigation, Methodology, Data curation, Writing – original draft, Experiments. **Hansol Lee:** Investigation, Experiments. **Jihoon Park:** Validation, Supervision, Writing – review & editing. **Jongryoul Kim:** Supervision, Funding acquisition, Project administration, Writing – review & editing.

Declaration of Competing Interest

The authors declare the following financial interests/personal relationships which may be considered as potential competing interests: Jongryoul Kim reports financial support was provided by Korea Evaluation Institute of Industrial Technology. Jongryoul Kim reports financial support was provided by National Research Foundation of Korea.

Data availability

Data will be made available on request.

Acknowledgements

This work was supported by the Korea Evaluation Institute Of Industrial Technology grant funded by the South Korea government the Ministry of Trade, Industry and Energy (Project Number: 20017593).

Also, this research was supported by Future Materials Discovery Program through the National Research Foundation of Korea (NRF) funded by the Ministry of Science and ICT (NRF-2021M3D1A2099404) and (NRF-2020M3H4A3082099).

Appendix A. Supplementary data

Supplementary data to this article can be found online at https://doi.org/10.1016/j.jmmm.2023.171327.

References

[1] J.M.D. Coey, Permanent magnets: Plugging the gap, Scr. Mater. 67 (2012) 524–529, https://doi.org/10.1016/j.scriptamat.2012.04.036.
[2] J. Park, Y.-K. Hong, J. Lee, W. Lee, S.-G. Kim, C.-J. Choi, Electronic Structure and Maximum Energy Product of MnBi, Metals 4 (2014) 455–464, https://doi.org/10.3390/met4030455.
[3] J. Cui, J.P. Choi, G. Li, E. Polikarpov, J. Darsell, N. Overman, M. Olszta, D. Schreiber, M. Bowden, T. Droubay, M.J. Kramer, N.A. Zarkevich, L.L. Wang, D. D. Johnson, M. Marinescu, I. Takeuchi, Q.Z. Huang, H. Wu, H. Reeve, N.V. Vuong, J.P. Liu, Thermal stability of MnBi magnetic Materials, J. Phys. Condens. Matter 26 (2014), 064212, https://doi.org/10.1088/0953-8984/26/6/064212.
[4] J.B. Yang, Y.B. Yang, X.G. Chen, X.B. Ma, J.Z. Han, Y.C. Yang, S. Guo, A.R. Yan, Q. Z. Huang, M.M. Wu, D.F. Chen, Anisotropic nanocrystalline MnBi with high coercivity at high temperature, Appl. Phys. Lett. 99 (2011), 082505, https://doi.org/10.1063/1.3630001.
[5] Y.-C. Chen, S. Sawatzki, S. Ener, H. Sepehri-Amin, A. Leineweber, G. Gregori, F. Qu, S. Muralidhar, T. Ohkubo, K. Hono, O. Gutfleisch, H. Kronmüller, G. Schütz, E. Goering, On the synthesis and microstructure analysis of high performance MnBi, AIP Adv. 6 (2016), 125301, https://doi.org/10.1063/1.4971759.
[6] Y.-K. Hong, J. Park, O.N. Mryasov, S.-G. Kim, S. Kim, J. Lee, G.S. Abo, C.-J. Choi, J. Lee, Magnetic properties of MnBi based alloys: First-principles calculations for MnBi-Co and MnBi-Co-Fe cases, AIP Adv. 3 (2013), 052137, https://doi.org/10.1063/1.4809564.
[7] J Köhler, J Kübler, Calculated magneto-optical properties of pure and doped MnBi, 1996 J. Phys.: Condens. Matter 8 8681. https://doi.org/10.1016/S0921-4526(97)00259-7.
[8] A. Sakuma, Y. Manabe, Y. Kota, First Principles Calculation of Magnetocrystalline Anisotropy Energy of MnBi and $MnBi_{1-x}Sn_x$, J. Phys. Soc. Jpn. 82 (2013), 073704, https://doi.org/10.7566/JPSJ.82.073704.
[9] P. Rania, A. Taya, M.K. Kashyap, Enhancement of magnetocrystalline anisotropy of MnBi with Co interstitial impurities, AIP Conf. Proc. 1942 (2018), 130033, https://doi.org/10.1063/1.5029103.
[10] Truong Xuan Nguyen, Hai Van Pham, Vuong Van Nguyen, Effect of Sb substitution on structural and magnetic properties of MnBi based alloys, Phys. B 552 (2019) 190, https://doi.org/10.1016/j.physb.2018.10.008.
[11] M. Choi, Y.-K. Hong, H. Won, G.J. Mankey, C.-D. Yeo, W. Lee, M.-H. Jung, T. Lee, J.-K. Lee, Suppressing antiferromagnetic coupling in rare-earth free ferromagnetic MnBi-Cu permanent magnet, J. Appl. Phys. 129 (2021), 113902, https://doi.org/10.1063/5.0040464.
[12] H.-D. Qian, Y. Yang, Jung Tae Lim, Jong-Woo Kim, Chul-Jin Choi, Jihoon Park, Effects of Mg and Sb Substitution on the Magnetic Properties of Magnetic Field Annealed MnBi Alloys, Nanomaterials 10 (11) (2020) 2265, https://doi.org/10.3390/nano10112265.
[13] Y. Yang, Jung Tae Lim, Jihoon Park, Nam-Kyu Kim, Hui-Dong Qian, Oi Lun Li, Jong-Woo Kim, Chul-Jin Choi, Effects of Sn addition on the microstructure and magnetic properties of MnBi bulk magnets, J. Alloy. Compd. 891 (2021), 161999, https://doi.org/10.1016/j.jallcom.2021.161999.
[14] V.V. Ramakrishna, S. Kavita, T. Ravi Gautam, R.G. Ramesh, Investigation of structural and magnetic properties of Al and Cu doped MnBi alloy, J. Magn. Magn. Mater. 458 (2018) 23–29, https://doi.org/10.1016/j.jmmm.2018.02.076.
[15] Y. Chen, C.P. Luo, Z.T. Guan, Q.Y. Lu, Y.J. Wang, The properties of magneto-optical MnBiY (Y = Al, Ag, Au, Cu, In, Zn, Pt) thin films, J. Magn. Magn. Mater. 115 (1992) 55–65, https://doi.org/10.1016/0304-8853(92)90183-O.
[16] S. Elena, Olivetti, Carmen Curcio, Luca Martino, Michaela Küpferling, Vittorio Basso, Effect of Ti substitution on α and β phase formation and properties in $Mn_{50-x}Ti_xBi_{50}$ alloys, J. Alloy. Compd. 643 (2015), https://doi.org/10.1016/j.jallcom.2014.12.060.
[17] P. Kharel, Ralph Skomski, R. D. Kirby, D. J. Sellmyer, Structural, magnetic and magneto-transport properties of Pt-alloyed MnBi thin films, J. Appl. Phys. 107, 09E303 (2010). https://doi.org/10.1063/1.3360204.
[18] P. Kharel, V.R. Shah, X.Z. Li, W.Y. Zhang, R. Skomski, J.E. Shield, D.J. Sellmyer, Structural and magnetic properties of Pr-alloyed MnBi nanostructures, J. Phys. D Appl. Phys. 46 (2013), 095003, https://doi.org/10.1088/0022-3727/46/9/095003.
[19] Y. Yang, J.-W. Kim, P.-Z. Si, H.-D. Qian, Y. Shin, X. Wang, J. Park, Oi Lun Li, Qiong Wu, Hongliang Ge, Chul-Jin Choi, Effects of Ga-doping on the microstructure and magnetic properties of MnBi alloys, J. Alloy. Compd. 769 (2018) 813–816, https://doi.org/10.1016/j.jallcom.2018.07.311.
[20] Y. Yang, Jung Tae Lim, Hui-Dong Qian, Jihoon Park, Jong-Woo Kim, Oi Lun Li, Chul-Jin Choi, Effect of Fe doping on the magnetic properties of MnBi alloy, J. Alloy. Compd. 855 (2021), 157312, https://doi.org/10.1016/j.jallcom.2020.157312.
[21] W. Zhang, B. Balasubramanian, P. Kharel, R. Pahari, S.a.R. Valloppilly, X. Li, L. Yue, R. Skomski, D.J. Sellmyer, High energy product of MnBi by field annealing and Sn alloying, APL Mater. 7 (2019), 121111, https://doi.org/10.1063/1.5128659.
[22] X. Guo, A. Zaluska, Z. Altounian, Ström-Olsen, J, The formation of single-phase equiatomic MnBi by rapid solidification, J. Mater. Res. 5 (11) (1990) 2646–2651, https://doi.org/10.1557/JMR.1990.2646.
[23] A.M. Gabay, G.C. Hadjipanayis, J. Cui, Preparation of highly pure α-MnBi phase via melt-spinning, AIP Adv. 8 (2018), 056702, https://doi.org/10.1063/1.5006491.
[24] K.W. Moon, K. Jeon, M. Kang, M. Kang, Y. Byun, J.B. Kim, H. Kim, J. Kim, Synthesis and magnetic properties of MnBi(LTP) magnets with high-energy product, IEEE Trans. Magn. 50 (2014) 1–4, https://doi.org/10.1109/TMAG.2014.2329555.
[25] A.M. Gabay, G.C. Hadjipanayis, J. Cui, Effect of Sb substitution on crystal structure, texture and hard magnetic properties of melt-spun MnBi alloys, J. Alloy. Compd. 792 (2019) 77–86, https://doi.org/10.1016/j.jallcom.2019.03.407.
[26] Xusheng Huang, Yuan Zhou, Wenwei Wu, Jiawei Xu, Shangqian Liu, Dongsheng Liu, Juan Wu, Effect of Zn^{2+} Substitution on the Structure and Magnetic Properties of $Co_{0.5}Cu_{0.5}Fe_2O_4$ Synthesized by Solvothermal Method, J. Electron. Mater. 45, 3113–3120 (2016). https://doi.org/10.1007/s11664-016-4400-1.
[27] L. Song, Y.u. Nengjun, M. Zhu, Q. Wang, W. Li, The microstructure and magnetization reversal behavior of melt-spun (Nd1-xCex)-Fe-B ribbons, J. Rare Earths 36 (2018), https://doi.org/10.1016/j.jre.2017.05.005.
[28] B.A. Jensen, W. Tang, X. Liu, A.I. Nolte, G. Ouyang, K.W. Dennis, J. Cui, Optimizing composition in MnBi permanent magnet alloys, Acta Mater. 181 (2019) 595–602, https://doi.org/10.1016/j.actamat.2019.10.003.
[29] X.F. Zhou, X.Z. Chen, Y.F. You, L.Y. Liao, H. Bai, R.Q. Zhang, Y.J. Zhou, H.Q. Wu, C. Song, F. Pan, Exchange Bias in Antiferromagnetic Mn_3Sn, Phys. Rev. Applied 14 (2020), 054037, https://doi.org/10.1103/PhysRevApplied.14.054037.
[30] H. Göbel, E. Wolfgang, H. Harms, Properties of MnBi compounds partially substituted with Cu, Zn, Ti, Sb, and Te. I. Formation of mixed phases and crystal structures, Phys. Status Solidi (a) 34, 553 (1976). https://doi.org/10.1002/pssa.2210340218.
[31] H. Göbel, E. Wolfgang, H. Harms, Properties of MnBi compounds partially substituted with Cu, Zn, Ti, Sb, and Te. II. Stability and magnetic properties of thin films, Phys. Status Solidi (a) 35(1):89-95 (1976). https://doi.org/10.1002/pssa.2210350110.
[32] A.F. Andresen, J.E. Engebretsen, Refsnes, Neutron Diffraction Investigations on Quenched MnBi and $MnBi_{0.9}Sb_{0.1}$, J Acta Chem. Scand. v26 p175 (1972), https://doi.org/10.3891/acta.chem.scand.26-0175.
[33] R.R. Heikes, Magnetic Transformation in MnBi, Phys. Rev. 99 (1955) 446, https://doi.org/10.1103/PhysRev.99.446.

[34] Trung Hieu Nguyen, Minh Tan Man, Hung Manh Do, Van Vuong Nguyen, Magnetic properties and electronic structure of the Sb-doped MnBi from DFT calculations, Solid State Commun. 336 (2021) 114385. https://doi.org/10.1016/j.ssc.2021.114385.

[35] Y.-C. Chen, G. Gregori, A. Leineweber, F. Quc, C.-C. Chen, T. Tietze, H. Kronmüller, G. Schütz, E. Goering, Unique high-temperature performance of highly condensed MnBi permanent magnets, Scr. Mater. 107 (2015) 131–135, https://doi.org/10.1016/j.scriptamat.2015.06.003.

[36] B. Li, Y. Ma, B. Shao, C. Li, D. Chen, JianChun Sun, Q. Zheng, X. Yin, Preparation and magnetic properties of anisotropic MnBi powders, Phys. B 530 (2018) 322–326, https://doi.org/10.1016/j.physb.2017.11.085.

[37] V. Ly, X. Wu, L. Smillie, T. Shoji, A. Kato, A. Manabe, K. Suzuki, Low-temperature phase MnBi compound: A potential candidate for rare-earth free permanent magnets, J. Alloy. Compd. 615 (2014) S285–S290, https://doi.org/10.1016/j.jallcom.2014.01.120.

[38] H. Sepehri-Amin, Y. Tamazawa, M. Kambayashi, G. Saito, Y.K. Takahashi, D. Ogawa, T. Ohkubo, S. Hirosawa, M. Doi, T. Shima, K. Hono, Achievement of high coercivity in Sm(Fe0.8Co0.2)12 anisotropic magnetic thin film by boron doping, Acta Mater. 194 (2020) 337–342, https://doi.org/10.1016/j.actamat.2020.05.026.

[39] X. Guo, X. Chen, Z. Altounian, J. O. Ström-Olsen, Magnetic properties of MnBi prepared by rapid solidification, Phys. Rev. B 46, 14578. https://doi.org/10.1103/PhysRevB.46.14578.

[40] J.B. Yang, W.B. Yelon, W.J. James, Q. Cai, S. Roy, N. Ali, Structure and magnetic properties of the MnBi low temperature phase, J. Appl. Phys. 91 (2002) 7866, https://doi.org/10.1063/1.1451306.

[41] Y.B. Yang, X.G. Chen, S. Guo, A.R. Yan, Q.Z. Huang, M.M. Wu, D.F. Chen, Y. C. Yang, J.B. Yang, Temperature dependences of structure and coercivity for melt-spun MnBi compound, J. Magn. Magn. Mater. 330 (2013) 106–110, https://doi.org/10.1016/j.jmmm.2012.10.046.